J. Fluid Mech. (1973), *vol.* 61, *part* 3, *pp.* 553–581
Printed in Great Britain

Nonlinear penetrative convection

By D. R. MOORE AND N. O. WEISS

Department of Applied Mathematics and Theoretical Physics,
University of Cambridge

(Received 23 March 1973)

Convection in water above ice penetrates into the stably stratified region above the density maximum at 4 °C. Two-dimensional penetrative convection in a Boussinesq fluid confined between free boundaries has been studied in a series of numerical experiments. These included cases with a constant temperature at both boundaries as well as cases with a fixed average flux at the lower boundary. Steady convection occurs at Rayleigh numbers below the critical value predicted by linear theory. At high Rayleigh numbers, resonant coupling between convection and gravitational modes in the stable layer excites finite amplitude oscillations. The problem can be described by a simplified model which allows for distortion of the mean temperature profile and balances the convected and conducted flux. This model explains the finite amplitude instability and predicts the Nusselt number as a function of Rayleigh number. These predictions are in excellent agreement with the computed results.

1. Introduction

In most laboratory experiments on convection the unstable layer is sandwiched between rigid boundaries. Stellar convection zones, on the other hand, are bounded by stably stratified regions and the penetration of convection across the interface between stable and unstable layers may be of astrophysical importance. For instance, solar granulation is actually observed in the stably stratified photosphere and may excite the oscillations that are detected in the atmosphere above. Penetrative convection may also affect nuclear abundances. For example, there is an apparent shortage of lithium in the sun and other late-type stars and it has been suggested that lithium is destroyed owing to slow mixing of material into the stable radiative zone.

A proper treatment of astrophysical, or indeed of meteorological, convection requires some understanding of the effect of relaxing the boundary conditions and of the qualitative features of penetrative convection (Spiegel 1972). Fortunately this can be gained from a simple experiment (Malkus 1960). The density of water is a maximum at 4 °C; thus, if a layer of water is maintained with its lower boundary at 0 °C and its upper boundary at some temperature greater than 4 °C, any convection in the lower, unstable region will penetrate into the stable layer above. This ice-water experiment has been carried out by Furumoto & Rooth (1961), Townsend (1964) and Myrup *et al.* (1970).

Veronis (1963) investigated the corresponding theoretical problem and found

a criterion for the onset of instability, analogous to that obtained by Rayleigh for Bénard convection (Chandrasekhar 1961). He also demonstrated that the system was unstable to finite amplitude disturbances at Rayleigh numbers less than the critical value predicted by linear theory, though he was not able to establish the lowest Rayleigh number for which steady-state convection could occur. This nonlinear behaviour was studied by Musman (1968), who solved the governing equations numerically in the mean-field approximation (Herring 1963; Spiegel 1967, 1971). He calculated the heat transport as a function of the Rayleigh number, estimated the critical Rayleigh number for the onset of nonlinear convection and also clarified Veronis's physical explanation of the finite amplitude instability.

In this paper we describe a simplified model of the ice-water problem which accurately predicts both the onset of nonlinear convection and the variation of the heat transport as the Rayleigh number is increased. We have also carried out detailed numerical experiments on two-dimensional penetrative convection. The results of these computations are analysed and compared with the simple model.

This model of steady penetrative convection is outlined in § 2. It allows for distortion of the mean temperature profile by convection, which causes the finite amplitude instability (Veronis 1963), and also uses the condition, first mentioned by Malkus (1963), that the total heat fluxes in the unstable and the stable layers must be equal.

The mathematical formulation of the problem, with the results of linear theory, is summarized in the next section. In § 4 we present the results of two-dimensional numerical experiments on steady penetrative convection between free boundaries at constant temperatures. These are first compared with results for Rayleigh–Bénard convection in order to establish the effect of replacing a material boundary by a 'soft' stable layer. The nonlinear instability, the heat flux and the extent of penetration are then investigated systematically. When the simple model is applied to this problem, the numerical results are predicted with remarkable accuracy.

At high Rayleigh numbers convection in the unstably stratified region excites gravitational oscillations in the stable layer above; these are described in § 5. After discussing the effects of varying the thermal boundary conditions, we compare our computations with laboratory experiments and finally review their astrophysical significance.

2. A simplified model calculation

The density of water around 4 °C is given approximately by the expression

$$\rho = \rho_0[1 - \alpha(T - T_0)^2], \tag{1}$$

where ρ is the density, T the temperature, T_0 the temperature at which the density is a maximum and α a constant coefficient of expansion. This expression holds to within 4 % over the range 0–8 °C; at standard pressure, $T_0 = 3{\cdot}98$ °C, $\alpha = 8{\cdot}0 \times 10^{-6}$ °K^{-2} and $\rho_0 = 1$ Mg m^{-3}. For the ice-water experiment we con-

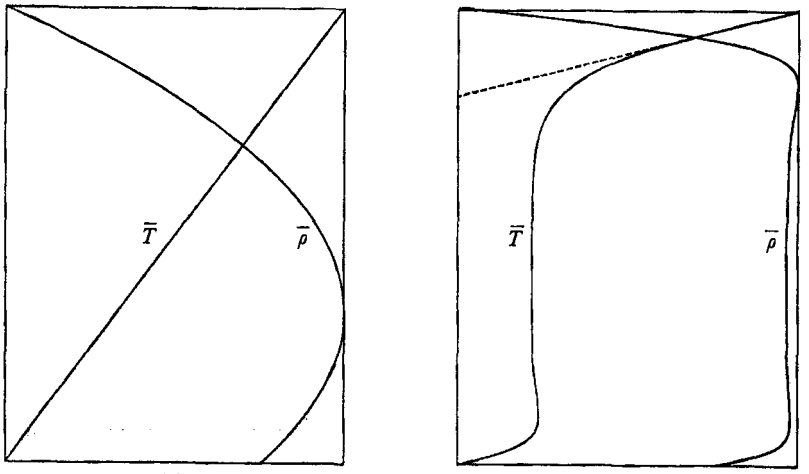

FIGURE 1. Penetrative convection, $\lambda = 3$; vertical profiles of mean temperature $\bar{T}$ and density $\bar{\rho}$. (*a*) Conduction only. (*b*) Convection at $R = 21R_c$.

sider an infinite plane layer of water of depth d, and measure temperature in °C. The lower boundary is kept at 0 °C and the upper boundary at a fixed temperature

$$T_U = \lambda T_0. \tag{2}$$

In the absence of motion the layer can only be in equilibrium if the vertical temperature gradient is constant, so that vertical profiles of T and ρ appear as shown in figure 1(*a*). The lower part of the layer is unstably stratified and we can measure the degree of instability by a Rayleigh number

$$\mathscr{R} = \frac{gd^3}{\kappa\nu}\left(\frac{\Delta\rho}{\rho_0}\right), \tag{3}$$

where $\Delta\rho$ is the density variation across the unstable region; here g is the gravitational acceleration, κ the thermometric conductivity and ν the kinematic viscosity. Thus, from (1) and (2), for $\lambda \geqslant 1$, the Rayleigh number is

$$R = g\alpha T_0^2 d^3/\kappa\nu. \tag{4}$$

The linear theory (Veronis 1963) tells us that the layer is unstable to infinitesimal perturbations only when R exceeds some critical value $R_c(\lambda)$. This can be estimated by calculating the effective Rayleigh number for the lower, unstable region of height d/λ,

$$R_0 = g\alpha T_0^2 d^3/\kappa\nu\lambda^3 = R/\lambda^3. \tag{5}$$

By analogy with Rayleigh–Bénard convection (Chandrasekhar 1961) we would expect a critical value for R_0 of order π^4; hence $R_c \sim \pi^4\lambda^3$. Veronis (1963) confirmed that $R_c \approx 2{\cdot}84\pi^4\lambda^3$ for $\lambda > 2$.

Once convection has set in, its efficacy can be measured as a normalized heat flux, the Nusselt number

$$N = Fd/\kappa\lambda T_0, \tag{6}$$

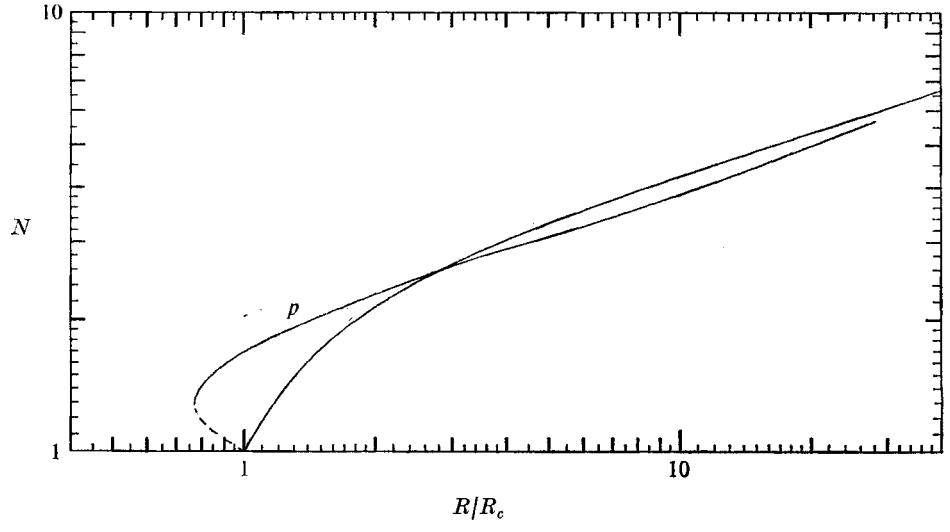

FIGURE 2. Heat flux as a function of Rayleigh number. For Rayleigh–Bénard convection the Nusselt number increases monotonically but the curve for penetrative convection with $\lambda = 3$ (labelled p) shows that convection can occur at subcritical Rayleigh numbers.

where F is the horizontally averaged downward thermometric flux. When heat is carried only by conduction $N = 1$, but $N > 1$ once steady convection has set in. For Rayleigh–Bénard convection $N = 1$ for all $R < R_c$, while the Nusselt number is continuous and increases monotonically with the Rayleigh number for $R > R_c$, as shown in figure 2. The corresponding curve for penetrative convection (obtained from numerical experiments with $\lambda = 3$) is quite different. The layer is unstable to finite amplitude disturbances for Rayleigh numbers less than the critical value predicted by linear theory: for a range of $R < R_c$ there are two stable solutions, one with $N = 1$ and the other with $N > 1$. As R is increased beyond R_c, the conducting solution becomes unstable and the Nusselt number jumps discontinuously to a higher value.

The existence of this nonlinear instability has a simple physical explanation (Veronis 1963; Musman 1968). Once convection occurs, the isotherms are distorted, as shown for instance in figure 7, and the unstable region penetrates into the level formerly occupied by stably stratified fluid. The overall effect of this penetration is shown by the mean temperature and density profiles in figure 1 (*b*): most of the fluid has a temperature less than T_0 and the stable region is crammed up near the top of the layer. Suppose that the convection cell penetrates to a height μd. Since the depth of the unstable region is now greater than for the conductive solution, $\lambda^{-1} < \mu < 1$. But the effective Rayleigh number for this unstable region is

$$R_E = g\alpha T_0^2 \mu^3 d^3/\kappa\nu = \mu^3 R \tag{7}$$

and $R_E > R_0$, the effective Rayleigh number for conductive equilibrium. Hence it is possible to maintain convection with R_E above its critical value when R_0 is still subcritical. Steady convection is therefore possible when the overall Rayleigh number R is less than the critical value R_c predicted by linear theory,

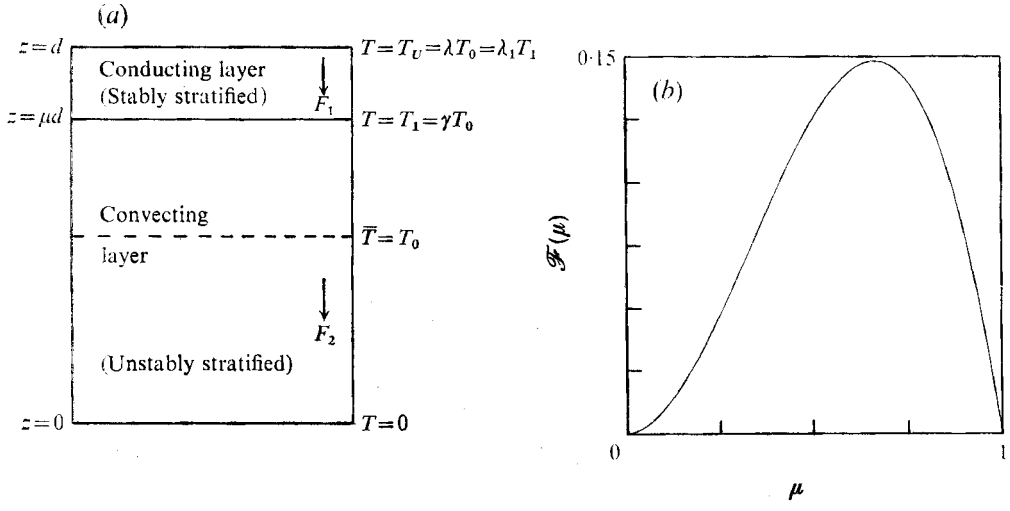

FIGURE 3. (*a*) Simplified model of penetrative convection.
(*b*) The function $\mathscr{F}(\mu) = \mu^2(1-\mu)$ for $0 < \mu < 1$.

although (for fixed R) this state can only be produced by a finite disturbance of the static equilibrium and a corresponding distortion of the mean density stratification. An analogous association between finite amplitude instabilities and distortions of mean fields is found in rotating systems or with thermosolutal convection (Veronis 1966*a*, 1965, 1968*a*,*b*).

Now convection penetrates into the stably stratified region with $T > T_0$. In the absence of any dissipation, buoyant fluid from the bottom of the layer could rise to the level where $T = 2T_0$ but the extent of penetration is reduced by thermal and viscous diffusivity. In fact, numerical experiments show that the boundary of the convective cell closely follows the 6° isotherm (see figure 7) while a weak counter cell appears above the convecting region. Let T_1 be the temperature of this interface; then we define a penetration factor γ such that

$$T_1 = \gamma T_0, \tag{8}$$

and assume that γ is independent of both R and λ. If z is the vertical co-ordinate and $\bar{T}(z)$ the horizontally averaged temperature then the depth of the unstable region is μd, where

$$\bar{T}(\mu d) = T_1. \tag{9}$$

Steady convection is possible only if the horizontally averaged heat flux F is independent of z. In the stably stratified region ($\mu d < z < d$) this flux is mainly by conduction, as in a thermal boundary layer; for $0 < z < \mu d$ the flux is mainly by convection. The condition that the fluxes in these two regions be equal can be used to determine the Nusselt number N as a function of R and, in particular, allows us to compute the minimum value of R for finite amplitude instability.

We shall therefore attempt to describe penetrative convection by the following simplified model. Consider a layer of depth d divided into two regions by a slippery plate at $z = \mu d$, maintained at a fixed temperature T_1, as shown in figure 3(*a*). In the upper, stably stratified region the heat flux is entirely by

conduction; in the lower, unstable region heat is carried by convection. We suppose that the position of the plate is adjusted until the heat fluxes above and below are equal and no external heating or cooling is required to maintain the temperature T_1.

In the upper, conducting region the thermometric flux

$$F_1 = \frac{\kappa(T_U - T_1)}{(1-\mu)d} = \frac{\lambda-\gamma}{1-\mu}\left(\frac{\kappa T_0}{d}\right). \tag{10}$$

In the lower region the ratio of the actual flux F_2 to the flux that would be carried in the absence of convection defines an effective Nusselt number

$$N_E = \frac{F_2 \mu d}{\kappa T_1} = \frac{\mu F_2}{\gamma}\left(\frac{d}{\kappa T_0}\right). \tag{11}$$

But convection extends throughout this region and the Nusselt number depends only on the Rayleigh number R_E defined by (7). So

$$N_E = \mathcal{N}(R_E/R_{Ec}), \tag{12}$$

where R_{Ec} is the critical value of R_E at the onset of convection and $\mathcal{N}$ is a function which can be determined by computation or experiment. For steady convection it is necessary that

$$F_1 = F_2 = F. \tag{13}$$

Then the overall Nusselt number

$$N = Fd/\kappa T_U = (\lambda-\gamma)/\lambda(1-\mu) \tag{14}$$

from (10), and from (10) and (11) the effective Nusselt number

$$N_E = (\lambda-\gamma)\mu/\gamma(1-\mu). \tag{15}$$

From (12) and (15), given the constant γ and the function $\mathcal{N}$, μ (and hence N) can be found as a function of R. It is then possible to describe the nonlinear instability and to predict the lowest Rayleigh number for which convection can occur.

Fortunately the qualitative features of penetrative convection can be illustrated by assuming a simple power-law relationship near the critical Rayleigh number such that

$$\mathcal{N}(R/R_c) = (R/R_c)^\beta, \tag{16}$$

where R is the relevant Rayleigh number and R_c its critical value for linear instability. Then

$$N_E = (R_E/R_{Ec})^\beta. \tag{17}$$

But $R_E = \mu^3 R$ and $R_{Ec} = (\gamma/\lambda)^3 R$, so

$$N_E = (\lambda_1\mu)^{3\beta}(R/R_c)^\beta, \tag{18}$$

where, for convenience, we define

$$\lambda_1 = \lambda/\gamma. \tag{19}$$

Then from (15) and (18) we obtain the equation

$$\mathcal{F}(\mu) \equiv \mu^{3\beta-1}(1-\mu) - \frac{\lambda_1 - 1}{\lambda_1^{3\beta}}\left(\frac{R_c}{R}\right)^\beta = 0. \tag{20}$$

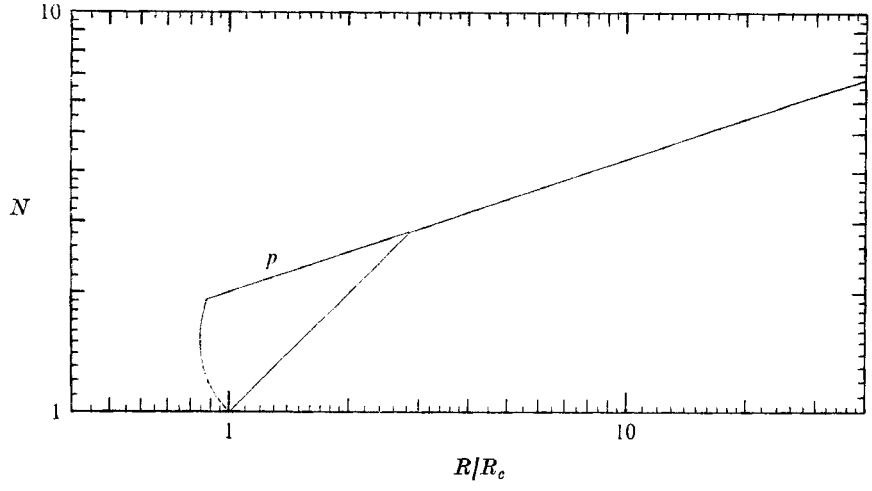

FIGURE 4. Crude model of penetrative convection. The crude power law (21) for Rayleigh–Bénard convection reduces to two straight lines. The curve labelled p shows the heat flux for penetrative convection, calculated from this law.

Now $\mathscr{F}(\mu) < 0$ when $\mu = 0, 1$ so long as $\beta > \frac{1}{3}$, and $d\mathscr{F}/d\mu = 0$ when

$$\mu = \mu_c = 1 - (3\beta)^{-1};$$

hence $\mathscr{F}(\mu)$ has a maximum in the range $0 < \mu < 1$ and (20) has two real solutions provided that $\mathscr{F}(\mu_c) > 0$. This determines the minimum Rayleigh number for which convection can occur.

The experimental results of Rossby (1969) for Rayleigh–Bénard convection in a layer with fixed boundaries can be represented by power laws valid over restricted ranges. Similarly, the computed heat flux for two-dimensional convection between free boundaries (Fromm 1965; Veronis 1966*b*; Moore & Weiss 1973) is roughly given by

$$\mathscr{N}(R/R_c) = \begin{cases} R/R_c & (1 < R/R_c < 2{\cdot}8), \\ 2(R/R_c)^{\frac{1}{2}} & (2{\cdot}8 < R/R_c < 50). \end{cases} \tag{21}$$

This crude law is plotted in figure 4 and the approximation involved can be assessed by comparison with the exact results in figure 2.

Let us therefore consider a crude model with $\beta = 1$. Then $\mathscr{F}(\mu)$ is a cubic which varies as shown in figure 3(*b*) and has a maximum at $\mu_c = \frac{2}{3}$. For a given value of R, equation (20) has in general two solutions, corresponding to two possible states of steady convection. However these solutions are real only if there exists some range of μ for which $\mathscr{F}(\mu) > 0$, for which it is necessary that

$$\mathscr{F}(\tfrac{2}{3}) = \tfrac{4}{27} - \frac{\lambda_1 - 1}{\lambda_1^3}\frac{R_c}{R} > 0, \tag{22}$$

or

$$R/R_c > \tfrac{27}{4}(\lambda_1 - 1)/\lambda_1^3. \tag{23}$$

This gives the minimum Rayleigh number for the occurrence of convection. Thus for $\lambda_1 > \frac{3}{2}$ the system is unstable to finite amplitude disturbances at Rayleigh numbers below the critical value predicted by linear theory.

When (23) is satisfied, convection can occur with two values of μ. The higher value is in the range $\frac{2}{3} < \mu < 1$: convection occurs over a relatively deep region and the stable layer is squeezed into a shallow region where conduction is effective. The alternative possibility has a thicker stable region and lower values of R_E and N. As μ diminishes the Rayleigh number increases, so that $R = R_c$ when $\mu = 1/\lambda_1$, and $R \to \infty$ as $\mu \to 0$.

The resultant convection is best described by expressing N as a function of R/R_c, using μ as a parameter. For instance, when $\lambda_1 = 2$ (e.g. $\lambda = 3$, $\lambda = \frac{3}{2}$)

$$N = \tfrac{1}{2}(1-\mu)^{-1}, \quad R/R_c = [8\mu^2(1-\mu)]^{-1} \tag{24}$$

and convection first sets in with $N = \frac{3}{2}$ and $R/R_c = 0{\cdot}84$. Values of N and R derived from (24) are plotted in figure 4, for comparison with the computed results in figure 2.

For fixed λ the parameter μ determines a unique family of possible equilibrium states with penetrative convection; there may, of course, be two such states for a given value of R. We now investigate the stability of these configurations by imagining that the interface between the conducting and convecting regions is free to move vertically without disturbing the fluid. Suppose that this surface $T = T_1$ is displaced upwards from its equilibrium position, so that more of the layer is at a lower temperature. Then the downward fluxes F_1 and F_2 will no longer be equal. If the conducted flux F_1 is greater than the flux F_2 convected away below the interface then the fluid around the interface will be heated and the surface $T = T_1$ will move downwards towards its equilibrium position (and vice versa). Now the simplified model depends only on the parameter μ and we assume therefore that the interface suffers a displacement $d\mu$ from its equilibrium position. Then a necessary condition for stability is that the flux difference $dF_1 - dF_2$ should have the same sign as $d\mu$, i.e. that $dF_1/d\mu > dF_2/d\mu$. But for the crude power law with $\beta = 1$, from (10), (11) and (18),

$$\frac{dF_1}{d\mu} - \frac{dF_2}{d\mu} = \frac{F_1}{1-\mu} - \frac{2F_2}{\mu} = \frac{(3\mu-2)F}{\mu(1-\mu)} \tag{25}$$

so the convective equilibrium is stable only if $\mu > \frac{2}{3}$, i.e. for the state with the greater Nusselt number.

From (21) the above treatment applies only for $N_E < 2{\cdot}8$ (though it could be adapted for any $\beta > \frac{1}{3}$). Thereafter, $N_E \propto R_E^{\frac{1}{3}}$ and N is a monotonically increasing function of R. In fact, when $N_E = c(R_E/R_{Ec})^{\frac{1}{3}}$ it follows from (14) and (20) that $N = c(R/R_c)^{\frac{1}{3}}$ too. Moreover, the heat flux

$$F = c\left(\frac{R}{R_c}\right)^{\frac{1}{3}} \frac{\kappa\lambda T_0}{d} \tag{26}$$

is independent of both λ and d, while the thickness of the upper thermal boundary layer is, from (14), also independent of d. These results, which apply quite generally for $R \gg R_c$, were first derived by Malkus (1963). The relationship between N and R derived from (21) for $R/R_c < 40$ is shown in figure 4 and can be compared with the corresponding curve in figure 2, obtained from numerical experiments.

So far we have concentrated on the simple power law (21) in order to explain the qualitative features of penetrative convection. However, a similar treatment can be carried through for an arbitrary $\mathscr{N}(R/R_c)$: for a given value of μ the equilibrium solution has a Nusselt number

$$N = (\lambda_1 - 1)/\lambda_1(1-\mu) \tag{27}$$

while the Rayleigh number can be obtained from

$$N_E = (\lambda_1 - 1)\,\mu/(1-\mu) = \mathscr{N}(\lambda_1^3 \mu^3 R/R_c). \tag{28}$$

This calculation is facilitated by a simple graphical construction, which will be described in §4.

Finally, the stability condition can be generalized. It is convenient to introduce the dimensionless flux difference

$$\Phi(R, \mu) = (F_1 - F_2)\, d/\kappa T_0. \tag{29}$$

Then the configuration is stable only if $\partial\Phi/\partial\mu > 0$. But

$$\left(\frac{\partial\Phi}{\partial\mu}\right)_R = -\left(\frac{\partial R}{\partial\mu}\right)_\Phi \left(\frac{\partial\Phi}{\partial R}\right)_\mu = -\frac{(\partial N/\partial\mu)_\Phi}{(\partial N/\partial R)_\Phi}\left(\frac{\partial\Phi}{\partial R}\right)_\mu \tag{30}$$

and

$$\left(\frac{\partial\Phi}{\partial R}\right)_\mu = -\left[\frac{\partial}{\partial R}\left(\frac{F_2 d}{\kappa T_0}\right)\right] < 0 \tag{31}$$

since $F_1 d/\kappa T_0$ depends only on μ. Moreover, for the equilibrium solutions $\Phi = 0$ and $dN/d\mu > 0$. So from (30), the stability condition is simply that $dN/dR > 0$. Indeed, Busse (1967*b*) has shown quite generally that convection in which the heat transport increases with decreasing Rayleigh number must be unstable. Thus we expect the family of solutions with $R < R_c$ and $dN/dR < 0$ to be unstable and unobtainable in practice. On the other hand, the purely conductive solution is stable for $R < R_c$ and the upper convective solution is always stable. For R less than the critical value for nonlinear convection only the conductive solution exists; for R between this value and R_c both the conductive solution and the upper convective solution are stable and any intermediate configuration must tend to one or other of these; and for $R > R_c$ only one convective solution is possible. The simple model therefore provides a qualitative explanation of all essential features of the finite amplitude instability.

Although this model can be fairly generally applied, we shall restrict our attention to two-dimensional convection between free boundaries, which can be accurately studied in numerical experiments. This problem will be systematically studied in the next four sections; in particular, we shall confirm that the simplified model is quite successful at predicting the results.

3. Equations and linearized theory

We consider two-dimensional convection in a Boussinesq fluid occupying the region $0 < x < L$, $0 < z < d$, so that all flow is confined to the x,z plane and independent of y. Then the velocity

$$\mathbf{u} = (u, 0, w) = (-\partial\psi/\partial z, 0, \partial\psi/\partial x), \tag{32}$$

where ψ is the stream function, and the vorticity has only a y component

$$\omega = -\nabla^2\psi. \tag{33}$$

The temperature T satisfies the heat flow equation

$$\partial T/\partial t = -\nabla.(T\mathbf{u}) + \kappa\nabla^2 T, \tag{34}$$

while the vorticity is governed by the equation

$$\frac{\partial\omega}{\partial t} = -\nabla.(\omega\mathbf{u}) - g\alpha\frac{\partial}{\partial x}T^2 + \nu\nabla^2\omega \tag{35}$$

(cf. Moore & Weiss 1973). We shall assume free boundaries, so the normal velocity and tangential stress both vanish at $z = 0, d$, and also that the stream function is an odd function of x and periodic. Then

$$\psi = \omega = 0 \quad (z = 0, d; \quad x = 0, L). \tag{36}$$

We also assume that the temperature is fixed on the horizontal boundaries, so

$$T = 0 \quad (z = 0), \quad T = \lambda T_0 \quad (z = d), \quad \partial T/\partial x = 0 \quad (x = 0, L). \tag{37}$$

Nonlinear penetrative convection can be studied by integrating (34) and (35) numerically, subject to boundary conditions (37) and (36), and then solving Poisson's equation (33) for ψ. The appropriate finite-difference techniques are described by Moore, Peckover & Weiss (1973) and their accuracy is also discussed by Moore & Weiss (1973). In all our numerical experiments the Prandtl number ν/κ was taken as 11·2, corresponding to water at 5 °C (Batchelor 1967, p. 597).

The stability of the static equilibrium solution with $T = \lambda T_0 z/d$ was investigated by Veronis (1963). It will prove convenient to summarize some results of linear theory here. For $\lambda < 1$ the Rayleigh number defined by (3) becomes

$$\mathscr{R} = g\lambda(2-\lambda)\alpha T_0^2 d^3/\kappa\nu \tag{38}$$

(Musman 1968) and as $\lambda \to 0$ the problem reduces to that of Rayleigh–Bénard convection. So instability first occurs when $\mathscr{R} = \frac{27}{4}\pi^4$ (as defined by (38)) and the normalized cell width

$$l = L/d \tag{39}$$

has the value $\sqrt{2}$ (Chandrasekhar 1961). Then the critical value of the Rayleigh number R defined by (4) is

$$R_c = 27\pi^4/4\lambda(2-\lambda) \tag{40}$$

and this expression holds to within 0·5 % for $\lambda \leqslant 1$.

For $\lambda > 1$ it is more convenient to use the Rayleigh number R_0 for the unstable region, defined in (5). Its critical value falls from $6{\cdot}72\pi^4$ when $\lambda = 1$ to a minimum of $2{\cdot}40\pi^4$ when $\lambda \approx 1{\cdot}7$; this drop is caused by the relaxation of the boundary conditions owing to the presence of a shallow stable layer. Shortly after the turning point, when $\lambda = 1{\cdot}9$, a counter cell appears in the stable region (Veronis 1963). For $1{\cdot}9 < \lambda < 3{\cdot}5$ the main cell has a single counter cell above it but another cell appears when $\lambda > 3{\cdot}5$. The critical value of R_0 rises to a slight subsidiary maximum at $\lambda \approx 2{\cdot}2$ and then settles down to an asymptotic value of $2{\cdot}84\pi^4$ for $\lambda > 2{\cdot}5$.

The temperature of the interface between the main cell and the first counter cell remains constant at $1{\cdot}48T_0$ for $\lambda > 1{\cdot}9$. Thus linear theory suggests that the temperature at the interface between the convecting and conducting regions $T_1 = 1{\cdot}5T_0$ and that the penetration factor $\gamma = 1{\cdot}5$. In order to describe the shape of the main convection cell, we take its height as $\mu_c d$, where $\mu_c = \gamma/\lambda$, and introduce an effective cell width $l_E = L/\mu d = l/\mu$. The value of l_E at which convection first appears drops from 1·41 to 1·37 when $\lambda = 1{\cdot}6$ and then to 1·15 when $\lambda = 1{\cdot}9$; thereafter it rises asymptotically to 1·24. We shall see later that the temperature at the interface between the main cell and the first counter cell, as well as the favoured cell width, is not significantly different for nonlinear convection.

4. Numerical experiments: steady convection

In the next three sections we present the results of a series of numerical experiments. First we consider steady laminar convection with fixed temperatures at the horizontal boundaries and describe the nonlinear instability. In §5 we discuss the time-dependent behaviour found at high Reynolds numbers and then, in §6, we investigate the effect of introducing a fixed-flux condition on one of the boundaries.

It is convenient to study convection as the Rayleigh number is varied for fixed values of λ. This corresponds to a sequence of experiments in which the temperature is held constant on the boundaries while the layer depth is varied; and we choose to express this depth in terms of the Rayleigh number $R \propto d^3$. Linear theory suggests that the results will depend on the value of λ: for $0 < \lambda < 1$ the whole layer is unstable and we can examine the effect of introducing a quadratic forcing term; for $1 < \lambda < 1{\cdot}91$ convection extends throughout the layer and we can study the influence of the soft boundary condition; and for $\lambda > 1{\cdot}91$ we can investigate the extent of penetration and the nonlinear instability. These problems will be treated in succession. We shall also see how accurately the simple model of §2 describes penetrative convection with $\lambda \geqslant 2$.

Effect of the forcing term ($0 < \lambda < 1$)

For Rayleigh–Bénard convection the density depends linearly on temperature. The quadratic dependence in (1) also reduces to a linear variation when $\lambda \ll 1$. When λ is small, therefore, convection above ice is indistinguishable from normal Rayleigh–Bénard convection, which has been discussed elsewhere (Moore & Weiss 1973). The difference between the quadratic and linear forcing terms grows as λ is increased. To investigate the effect of this difference the Nusselt number was found for a range of Rayleigh numbers with $\lambda = 1$ and the results are plotted in figure 5, together with a couple of cases for $\lambda = \frac{1}{3}$ and $\frac{2}{3}$. All calculations were done with a normalized cell width $l = \frac{4}{3}$, using a square mesh with 24×18 intervals. The Nusselt numbers for ice-water and Rayleigh–Bénard convection are indistinguishable. However, a close comparison of the streamlines and isotherms for $\lambda = 1$ and $R = 20R_c$ in figure 6 reveals some differences. The fields are no longer symmetric about the centre of the cell: the

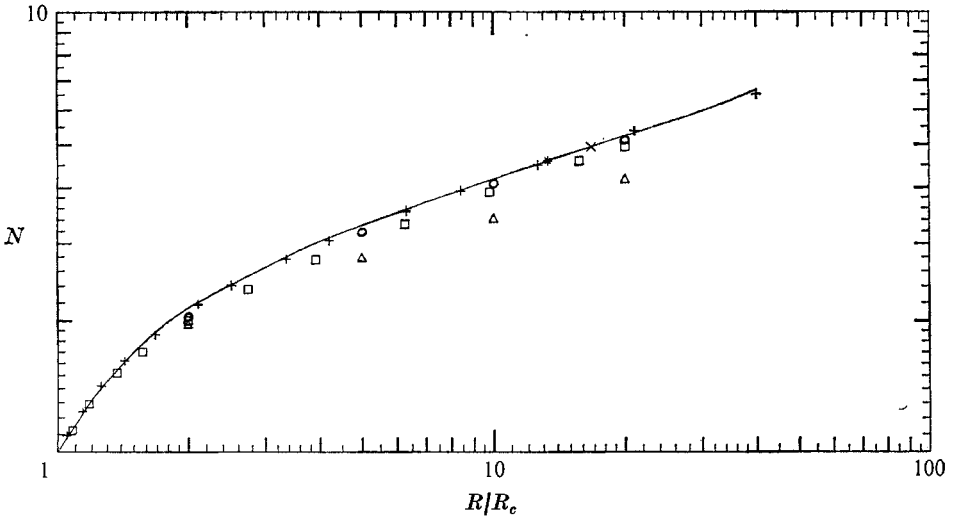

FIGURE 5. The effect of the quadratic forcing term and the upper boundary condition. N as a function of R. $\times$, $\lambda = \frac{1}{3}$; $*$, $\lambda = \frac{2}{3}$; $+$, $\lambda = 1$; $\bigcirc$, $\lambda = 1{\cdot}25$; $\square$, $\lambda = 1{\cdot}5$; $\triangle$, $\lambda = 1{\cdot}75$; ——, results for Rayleigh–Bénard convection.

rising plume of cooler fluid is narrower, while the descending flow is significantly broader and the stagnation point is shifted towards the rising plume.

In general these results suggest that the form of the forcing terms may alter the local structure of the flow but does not affect the overall heat transport. Any observed differences in Nusselt number between penetrative and classical convection must be produced by the stable layer above.

Effect of the boundary conditions ($1 < \lambda < 1{\cdot}91$)

When $\lambda > 1$ the horizontally averaged temperature $\overline{T}(z)$ is stably stratified near $z = d$ but for $\lambda < 1{\cdot}91$ the convection cell fills the whole layer. The change in the form of the motion as λ increases is shown in figure 6. Streamlines and isotherms are plotted for $\lambda = 1$, 1·5 and 2 with $R = 20R_c$. The asymmetry develops as λ increases but there is no striking change until the counter cell appears. For $\lambda < 1{\cdot}6$ the most unstable mode (with $l \sim \sqrt{2}$) is also the most efficient at moderate Rayleigh numbers.

In figure 5 the Nusselt number is plotted as a function of R/R_c for $\lambda = 1{\cdot}25$, 1·5 and 1·75 and compared with the results for $\lambda = 1$. The dependence is similar, though the efficiency of convection decreases slightly as λ is increased: for $R > 5R_c$, $N = c(R/R_c)^{\frac{1}{3}}$ and $c = 1{\cdot}96$ for $\lambda = 1$ (as for Rayleigh–Bénard convection) but when $\lambda = 1{\cdot}25$, 1·5 and 1·75 c drops to 1·87, 1·83 and 1·60 respectively. This decrease is caused by the need to drive the motion through the stably stratified region near the upper boundary.

The fall in the critical Rayleigh number compensates for this apparent loss of efficiency and the change in R_c is caused by the soft fluid boundary, which permits the isotherms to assume a more efficient shape for convection. The relaxation of constraints on the velocity seems to be more important than any change in the thermal boundary conditions. The effect of horizontal temperature variations

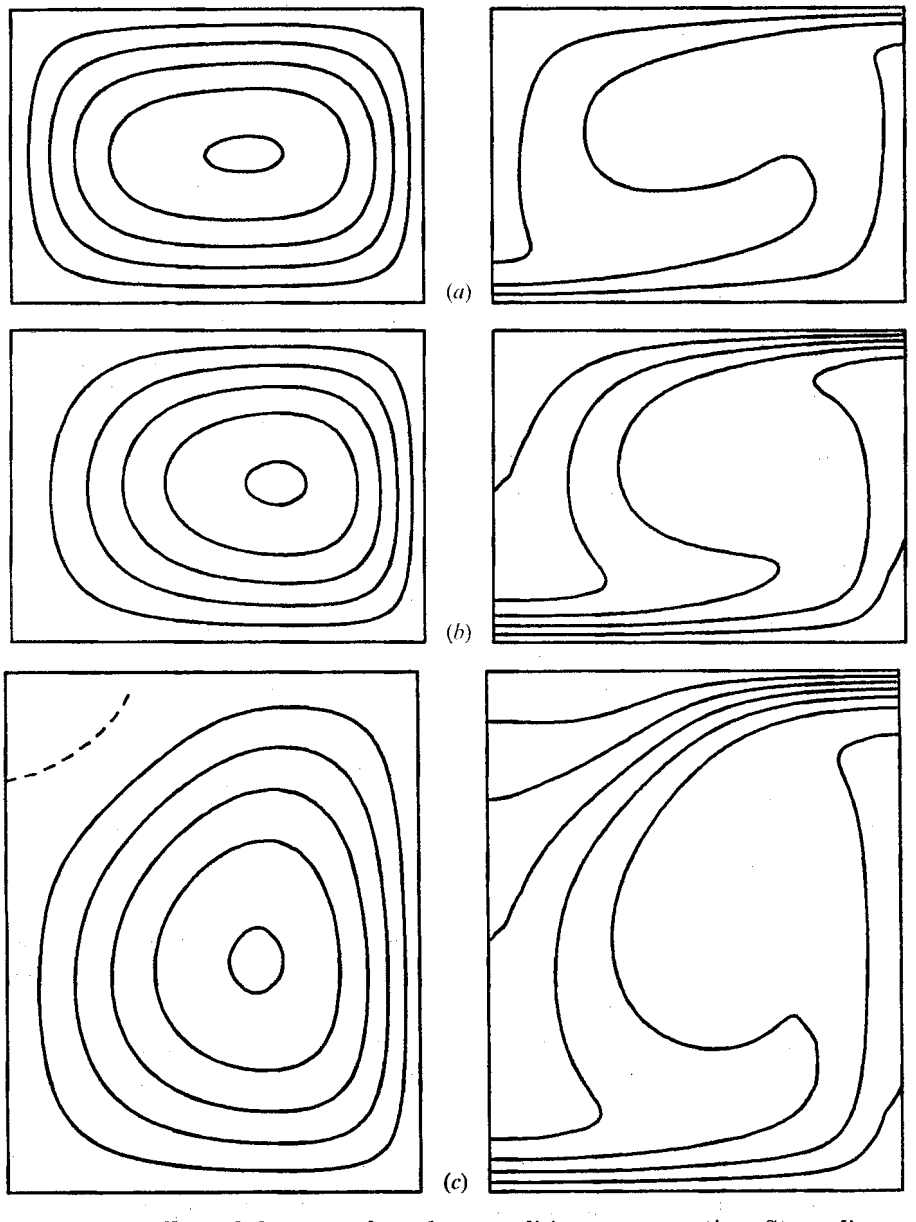

FIGURE 6. The effect of the upper boundary condition on convection. Streamlines and isotherms for $R = 20R_c$. (*a*) $\lambda = 1$, (*b*) $\lambda = 1{\cdot}5$, (*c*) $\lambda = 2$. As λ increases, the isotherms become increasingly asymmetric, and a small counter cell appears. The broken line separates the main cell from the counter cell and isotherms are drawn at intervals of 1 °C, with the lower boundary at 0 °C.

along the upper boundary was investigated in a number of runs at $R = 2R_c$ with $T(x, d) = 1{\cdot}5T_0(1 + \delta \cos \pi x/L)$ and $0 \leqslant \delta \leqslant 1$. The Nusselt number decreases from 2·00 when $\delta = 0$ to 1·99 when $\delta = 0{\cdot}2$ and 1·83 when $\delta = 1$. Thus N is primarily dependent on the mean temperature of the upper boundary; this is convenient for the simple model of §2.

Penetrative convection ($\lambda > 1{\cdot}91$)

The streamlines for $\lambda = 2$ in figure 7 show a small counter cell in the stable region. This first appears when $\lambda = 1{\cdot}91$, and becomes more prominent when $\lambda = 3$, as shown in figure 7(*a*). Thus convection no longer penetrates to the upper boundary and the fluid can be divided into a convecting region (of average height μd) and a stable conducting layer above it. Figure 2 displays the striking change in the variation of N with R/R_c. When $\lambda = 6$ the stable region has grown larger and a second, feebler counter cell has appeared, as shown in figure 7(*b*). As λ is increased, convection appears with finite amplitude at smaller subcritical Rayleigh numbers. The value of R/R_c for which N becomes proportional to $R^{\frac{1}{3}}$ also decreases. This behaviour is explained by the simple model of §2.

Mean temperature profiles for various Rayleigh numbers at $\lambda = 3$ are shown in figure 8. The temperature gradient is linear near the upper boundary and the temperature at the interface between the conducting and convecting region varies between 5° and 8 °C. Inspection of the streamlines and isotherms shows that this boundary approximately follows an isotherm whose temperature varies between $1{\cdot}25T_0$ at small Rayleigh numbers and $1{\cdot}75T_0$ when $R/R_c = 20$. Although there is a temperature variation of about $0{\cdot}2T_0$ along the interface this should have little effect on the heat transport. We shall therefore assume that the interface occurs at a fixed temperature $T_1 = 1{\cdot}5T_0$ and that the penetration factor $\gamma = 1{\cdot}5$. Linear theory satisfactorily predicts both this interface and the cell width that maximizes the heat flux.

We can now compare the computed results with the simplified model described in §2, taking $\gamma = 1{\cdot}5$. In order to apply the model we also need to know the effective Nusselt number

$$N_E = \mathcal{N}(R_E/R_{Ec}) \tag{41}$$

for the convecting region. For this we adopt the function $\mathcal{N}$ obtained with $\lambda = 1{\cdot}5$, which is shown in figure 9. The results of this single run, combined with the simple model, can then be used to predict the Nusselt number for all $\lambda > 1{\cdot}5$. For any value of λ, N and R can be calculated, using μ as a parameter, as described in §2. However, the following graphical procedure is more informative and appealing.

From (28),

$$\mu = N_E/(\lambda_1 - 1 + N_E), \tag{42}$$

where $\lambda_1 = \lambda/\gamma$, and μ can therefore be eliminated from (27) to give

$$N = (\lambda_1 - 1 + N_E)/\lambda_1. \tag{43}$$

Also,

$$\frac{R}{R_c} = \frac{1}{(\lambda_1\mu)^3}\frac{R_E}{R_{Ec}} = \left(\frac{\mu_c}{\mu}\right)^3 \frac{R_E}{R_{Ec}} = \left(\frac{N}{N_{\hat{E}}}\right)^3 \frac{R_{\hat{E}}}{R_{Ec}}, \tag{44}$$

where μ_c is the value of μ for the state of marginal stability. Let us now define new variables

$$X = \mu^3, \quad Y = N_E/(\lambda_1 - 1). \tag{45}$$

Then (27), which expresses the balance between convective and conductive flux, becomes

$$Y = X^{\frac{1}{3}}/(1 - X^{\frac{1}{3}}). \tag{46}$$

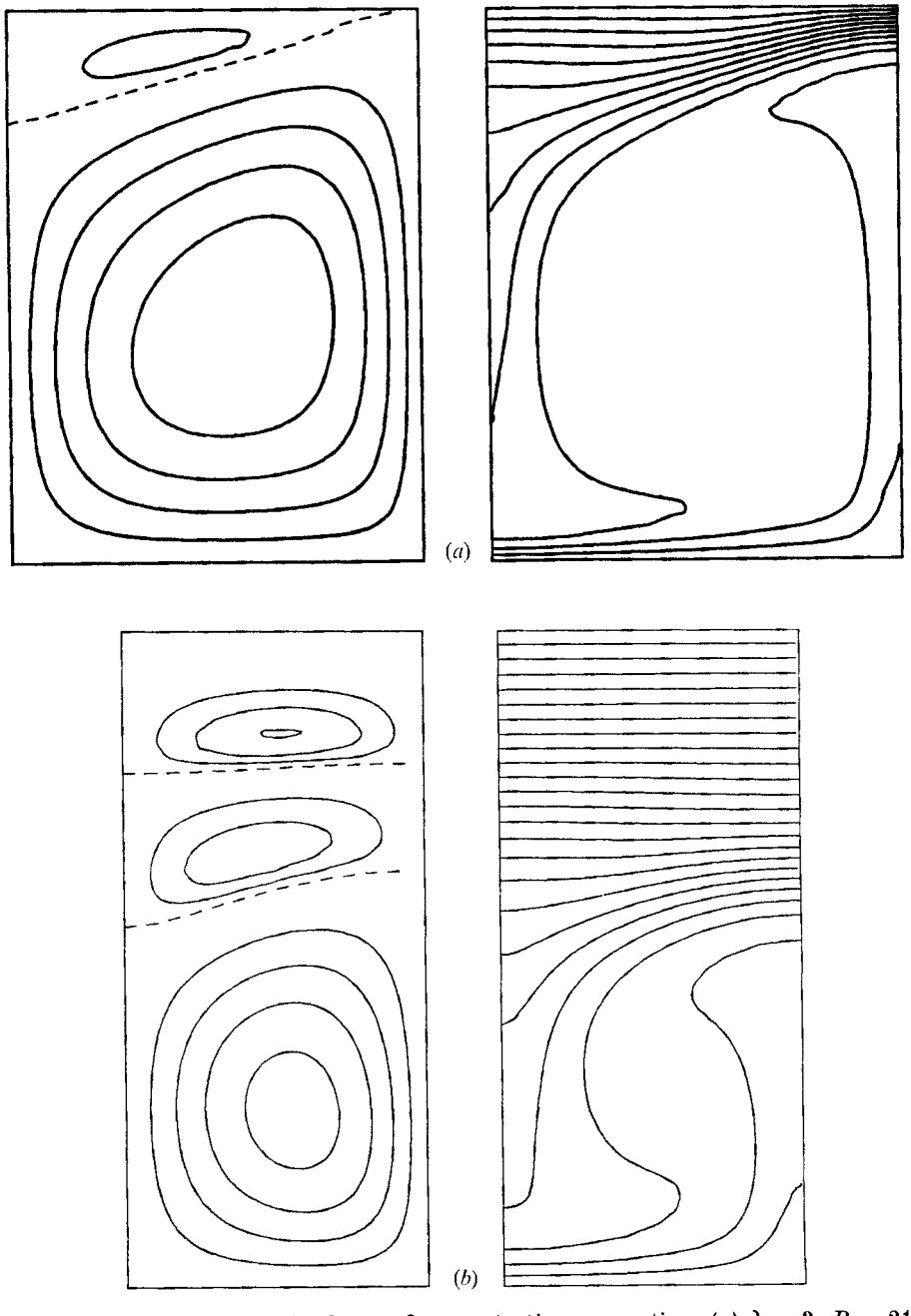

FIGURE 7. Streamlines and isotherms for penetrative convection. (*a*) $\lambda = 3$, $R = 21R_c$: there is a single counter cell in the stable region. (*b*) $\lambda = 6$, $R = R_c$: two counter cells are formed (the intervals between streamlines in the main cell and the first and second counter cells are in the ratio 1:0·15:0·01).

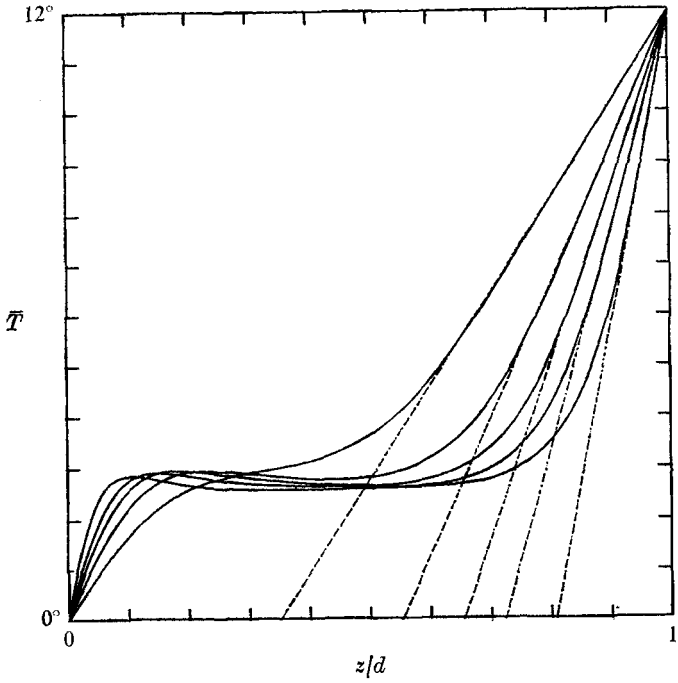

FIGURE 8. Mean temperature profiles for penetrative convection, $\lambda = 3$: $\bar{T}$ as a function of z/d. The broken lines give the slope at $z = d$ for (from left to right) $R/R_c = 0{\cdot}88$, 1·76, 3·51, 7·02, 21·05.

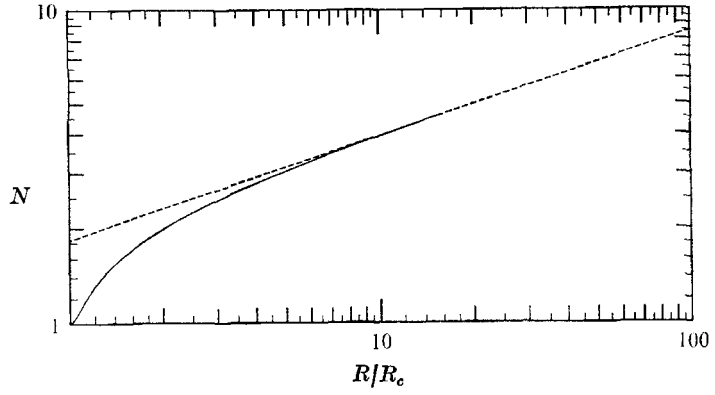

FIGURE 9. Logarithmic plot of N as a function of R/R_c for $\lambda = 1{\cdot}5$. The dashed line corresponds to $N \propto R^{\frac{1}{3}}$ and is fitted to the result for $R = 10R_c$.

Figure 10 is a logarithmic plot of $Y(X)$, using the same scales as figure 9. To find the Nusselt number we place a transparent copy of figure 9 on top of figure 10 with the line $N_E = 0$ above the line $Y = Y_0 = (\lambda_1 - 1)^{-1}$. We can then slide the transparency from right to left along this line until the curve of $\mathcal{N}(R/R_c)$ intersects that of $Y(X)$.

Various types of behaviour are possible. There is a range of positions for which $Y > \mathcal{N}$ and the curves do not cross. This corresponds to values of R/R_c for

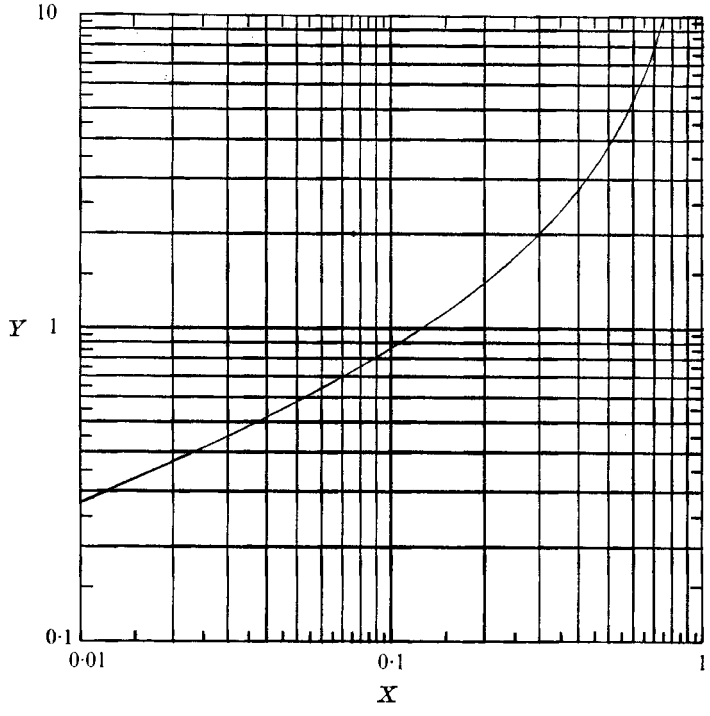

FIGURE 10. Logarithmic plot of the function $Y = X^{\frac{1}{3}}/(1-X^{\frac{1}{3}})$, on the same scale as figure 9.

which there is no convecting solution and only the trivial conducting solution with $\mathcal{N} = 1$. As the transparency is slid to the left, R/R_c is increased until $\mathcal{N}(R_E/R_{Ec})$ touches $Y(X)$. This point marks the onset of nonlinear convection and exists for $\mathcal{N} > 1$ so long as $\lambda_1 > 1{\cdot}25$ ($\lambda > 1{\cdot}9$). It is followed by a region where the graphs intersect at two points, representing two possible convective solutions, of which only the upper one is stable. The lower point of intersection moves down the curves until it reaches the point $N_E = 1$, $R_E/R_{Ec} = 1$: this corresponds to the onset of linear instability, where $Y = (\lambda_1 - 1)^{-1}$ and $X = X_0 = \mu_c^3$. From then on, there is only one convective solution, given by the upper point of intersection.

The effective Nusselt number N_E is read directly from the upper graph and N must be calculated from (43). From (44), $R/R_c = (X_0/X)\, R_E/R_{Ec}$ and so R/R_c is simply given by the value of R_E/R_{Ec} at X_0 (if $R/R_c \geqslant 1$) or by letting the line $R_E/R_{Ec} = 100$ run through the point of intersection and reading off $100R/R_c$ as the abscissa of the point X_0 (when $R/R_c < 1$).

The model can thus be used to predict the minimum value r_0 of R/R_c for which convection can occur and the corresponding value of the Nusselt number, as well as the value r_1 of R/R_c at which N becomes proportional to $R^{\frac{1}{3}}$. These predictions are listed in table 1. The predicted relationships between N and R/R_c for $\lambda = 2$, 3 and 6 are shown in figure 11, together with values calculated from numerical experiments. They are in excellent agreement. We therefore

λ	λ_1	Y_0	r_0	r_1	Nusselt number, N $R/R_c = r_0$	$R/R_c = 1$
			(*a*) *Free boundaries*			
2	1·33	3	0·98	3·3	1·12	1·25
3	2	1	0·78	2·0	1·28	1·69
6	4	0·333	0·49	1·0	1·28	1·83
12	8	0·143	0·33	0·81	1·14	1·82
			(*b*) *Rigid boundaries*			
3	2	1	0·89	—	1·14	1·33
6	4	0·333	0·62	—	1·15	1·32

TABLE 1. Predicted Nusselt and Rayleigh numbers

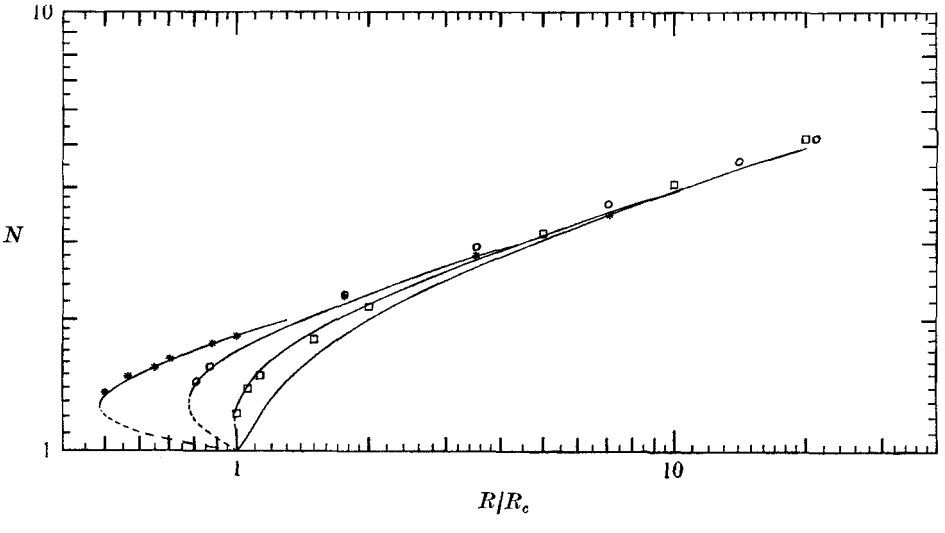

FIGURE 11. Comparison between the model and the results of numerical experiments. The curves show predicted values of N for $\lambda = 1{\cdot}5, 2, 3, 6$. They are in excellent agreement with the computed points. □, $\lambda = 2$; ○, $\lambda = 3$; ∗, $\lambda = 6$.

conclude that the model of §2 provides a satisfactory description of penetrative convection.

The streamlines and isotherms in figures 6 and 7 are definitely skew, while the model assumes a unique value of μ. However, the heat flux in the stable region depends only on the average temperature gradient and we have shown that the energy carried by a convection cell is insensitive to horizontal variations of temperature on its upper boundary. The overall heat flux is also insensitive to the slow increase of γ with R (Malkus 1963). Thus the Nusselt number can be accurately predicted.

Our numerical results also confirm the estimates of critical cell widths and Rayleigh numbers described in §3. When the uniformly stratified temperature was randomly perturbed by 0·01% of its value the perturbations decayed for $R < R_c$ but grew exponentially when $R > R_c$. The nonlinear convective states

had to be started from velocity and temperature fields obtained with $R > R_c$. When these were used as initial values for subcritical Rayleigh numbers the results converged to the expected steady state. As R was decreased, convergence became slower. For Rayleigh numbers below the critical value for nonlinear convection, all disturbances rapidly decayed. As expected, the second convective solution proved unstable: attempts to set it up evolved to either the conductive or the more efficient convective solution. (This second solution can be stabilized by modifying the boundary conditions and its existence is demonstrated in §6.)

Musman (1968) computed similar results, using the mean-field approximation, which overestimates the heat flux (Deardorff 1964; Elder 1969). Consequently he found a higher penetration factor ($\gamma = 1{\cdot}75$) and predicted that finite amplitude convection would be possible at much lower Rayleigh numbers ($R/R_c = 0{\cdot}35$ for $\lambda = 3$) than we have found in our two-dimensional computations. Comparison of our stream functions and isotherms with those in his paper reveals several differences. The stream function is symmetrical about $x = \frac{1}{2}L$ in the mean-field approximation and convection cells are therefore rectangular, whereas the nonlinear relationship between ρ and T leads to penetration by the rising plumes in our numerical experiments, where the distorted streamlines correspond to a trapezoidal cell. Closed isotherms (which are not permissible in a steady solution of (34)) are absent in the two-dimensional results while the soft upper boundary condition enhances the temperature difference in the wide sinking plume. So the discrepancies between Nusselt numbers for two-dimensional penetrative convection found from (33)–(35) and those calculated from the mean-field equations are scarcely surprising. Nevertheless, the latter, given appropriate values of γ and $\mathcal{N}(R/R_c)$, are still consistent with the simple model.

5. Time-dependent behaviour

The time-dependent behaviour of the numerical models changes drastically as the Rayleigh number is increased. With $\lambda = 3$, the results converge monotonically to a steady solution, at a rate determined by the thermal time scale for the stable region, for $R < 5R_c$. For $5 < R/R_c < 10$, the Nusselt number oscillates about its final value with an amplitude that decays exponentially at the same rate. At higher Rayleigh numbers convergence becomes increasingly slow: for $R = 28R_c$ the amplitude of variations in the Nusselt number falls by a factor of e after about 30 oscillations, corresponding to the thermal decay time for the whole layer. When R is further increased, finite amplitude oscillations persist indefinitely. Analogous behaviour is found when $\lambda = 6$. In order to confirm that the oscillations were not a result of some numerical instability caused by inadequate resolution of the boundary layer the number of mesh intervals was increased from 64 to 128: the oscillations persisted, with the same period but a slightly larger amplitude.

Similar oscillations were found in the experiments of Townsend (1964) and Myrup *et al.* (1970). Townsend demonstrated that the period of the oscillations was consistent with their being gravity waves in the stably stratified layer,

excited by irregular convection from below. Musman (1968) also found oscillations which impaired the convergence of his iterative method and suggested that these might correspond to gravitational modes.

The nonlinear oscillations mainly affect the region $z \gtrsim \mu d$ and are most pronounced around the interface between the stable and unstable layers. Their general pattern can be seen from the sequence of streamlines and isotherms in figure 12, for $\lambda = 3$ and $R = 42R_c$. The interface tips to and fro as colder or warmer fluid circulates around the convection cell. Thus the oscillations are produced by a nonlinear resonant coupling between fluctuations in convective penetration from below and internal gravity waves above. An abnormally cold blob of fluid penetrates further into the stable layer; as it moves from side to side across the interface, the oscillation must change in phase by π, so the period of the oscillation should be half the turnover time for the cell. This is confirmed by the results in table 2. For $R < 20R_c$, the approximate turnover time (measured in dimensionless units) is roughly equal to the period of the damped oscillations but when $R > 20R_c$ oscillations appear with a period equal to half the estimated turnover time.

Resonance will occur if this turnover time is twice the period of a normal mode for the stable region. For a horizontally stratified region with a uniform temperature gradient, the frequency ω can be found by solving Airy's equation as an eigenvalue problem (Townsend 1964). We shall only consider a simplified model with $d\rho/dz$ constant. Then the fundamental mode has a vertical velocity

$$w \propto \frac{m\pi z}{(1-\mu)d} \exp i\left(\omega t + \frac{\pi x}{L}\right) \tag{47}$$

and the dispersion relation (Lamb 1932, p. 378) becomes

$$\omega^2 = -g\left[1 + \frac{l^2m^2}{(1-\mu)^2}\right]\frac{1}{\rho}\frac{d\rho}{dz}, \tag{48}$$

so that for $\lambda = 3$ and $\gamma = \frac{3}{2}$ the period

$$\tau_G = \left(\frac{d}{g\alpha T_0^2}\right)^{\frac{1}{2}} \tau'_G = \left(\frac{d}{g\alpha T_0^2}\right)^{\frac{1}{2}} \left[\frac{1 + 4l^2m^2N^2}{6N(T/T_0 - 1)}\right]. \tag{49}$$

For the model shown in figure 3, $R = 21R_c$, $l = \frac{3}{4}$ and $N = 5{\cdot}2$. The dimensionless periods τ'_G estimated at the base, midpoint and top of the stable region for $m = \frac{1}{2}$ are 9·16, 5·80 and 4·60 respectively; the corresponding values for $m = 1$ are 17·7, 11·62 and 8·88; and the periods obtained from Airy's equation must lie within these ranges. Since the oscillation is driven from below, the boundary $z = \mu d$ should resemble an antinode. Yet the observed dimensionless period of 10·0 lies outside the range for $m = \frac{1}{2}$. There are two reasons for this discrepancy: first, the proper boundary conditions are more complicated; second, the layer is not horizontally stratified. Thus the period cannot be predicted by simple arguments based on (47).

Without some excitation mechanism the oscillations decay through viscous and thermal dissipation. Oscillatory behaviour was described by Welander

(1967) for a simple model of convection and found by Moore & Weiss (1973) in numerical experiments on Rayleigh–Bénard convection: when the width was inappropriately chosen, three hot and three cold blobs circulated alternately around the cell. The oscillations found with penetrative convection are qualitatively different. As can be seen from figure 12, only two pairs of hot and cold blobs are present and the most striking changes are in the stable region. The vigorous rising plume compresses the non-convecting region until the counter cell has disappeared and cold fluid spreads across the upper portion of the cell. The coupling between temperature and circulation speed is sufficient to maintain the oscillation. The horizontally averaged heat transport, also plotted in figure 12, shows the dominance of the rising plume: the Nusselt number at $z = \frac{5}{6}$ varies from $-0{\cdot}5$ to 17, while at that the boundary fluctuates between 4·8 and 8·4.

Coupling between the stable and unstable regions is necessary for oscillations to persist and the resonance peak is likely to be very broad. For large Rayleigh numbers the turnover time $\tau_0' \propto R^{-\frac{1}{3}}$ (Moore & Weiss 1973) while, from (49), the oscillation period $\tau_G' \propto N^{\frac{1}{2}} \propto R^{\frac{1}{4}}$. As the stable layer grows thinner, its period becomes longer and so the resonance should ultimately disappear. Over the range that we have investigated the amplitude of the oscillations apparently increases with R. However, we have only varied the Rayleigh number by a factor of two and the asymptotic behaviour remains unclear.

There is a general resemblance between oscillations of the stable region in our two-dimensional model and in Townsend's experiment but the exciting mechanisms are as different as a fiddle and a drum. In the numerical experiments there is a forced gravitational resonance, driven by the periodic convective circulation. On the other hand, the laboratory experiments show free oscillations of the stable region, excited randomly by thermals impinging on the interface. This latter mechanism has more geophysical and astrophysical relevance.

6. Fixed-flux boundary conditions

Astrophysical convection is more closely approximated by a configuration in which the heat flux, rather than the temperature, is prescribed on the lower boundary. This variation can easily be included in computational models. For comparison with the cases described above it is convenient to maintain a uniform temperature T_L at the lower boundary, which varies with time in such a way that the mean heat flux is constant. Since this flux is all by conduction, the boundary condition (37) is replaced by

$$d\bar{T}/dz = \text{constant} \ (z = 0), \quad T = \lambda T_0 \ (z = d), \quad \partial T/\partial x = 0 \ (x = 0, L; z = 0). \tag{50}$$

This change stabilizes all convective solutions and so allows us to investigate the lower range of nonlinear solutions (indicated by dashed lines in figure 11) for $r_0 < R/R_c < 1$. For consider an equilibrium solution represented by the simplified model of §2 and suppose that the interface where $T = T_1$ suffers a displacement $d\mu$. Then the lower temperature has to adjust itself so that the

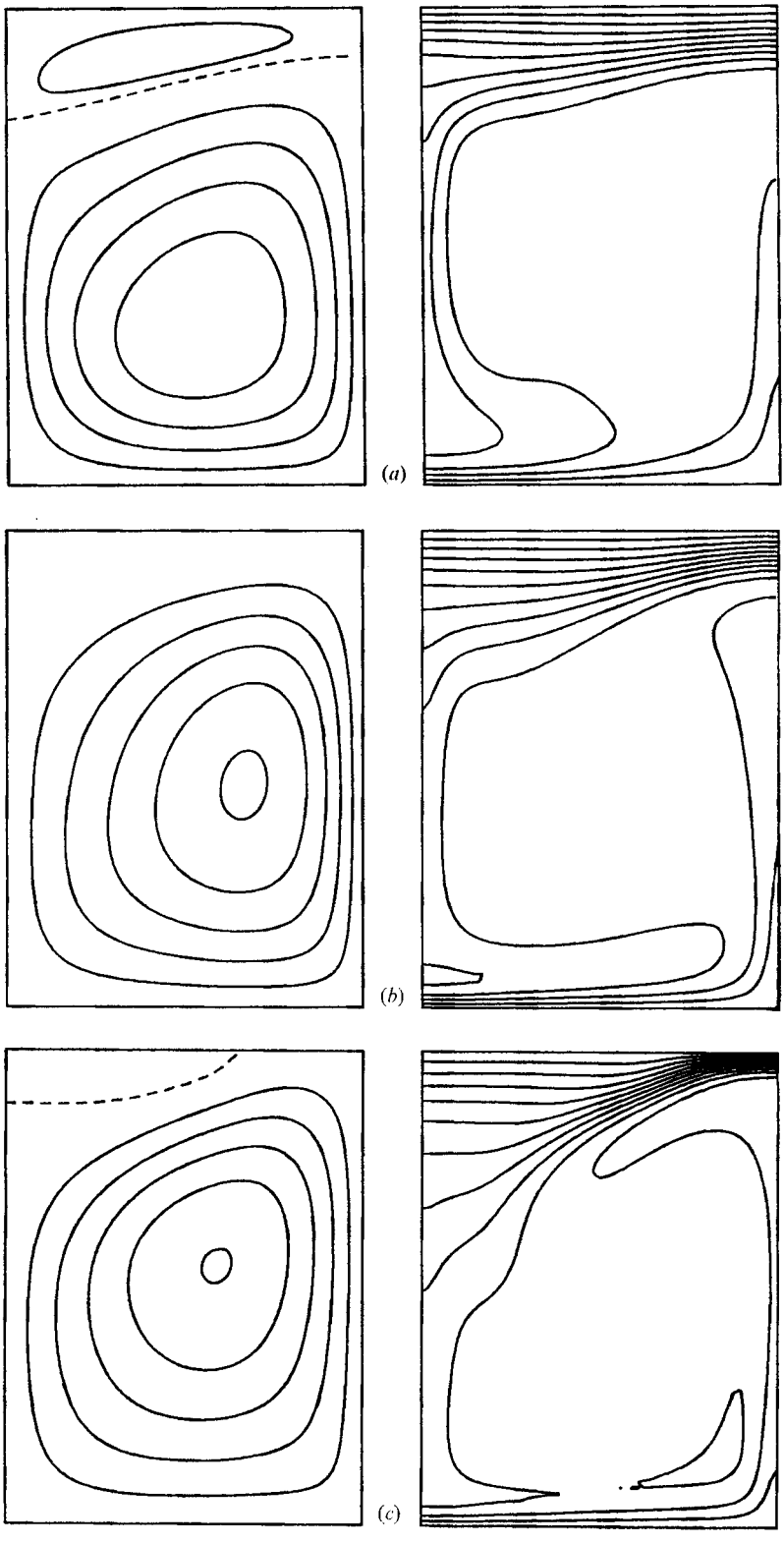

FIGURES 12 (*a–c*). For legend see facing page.

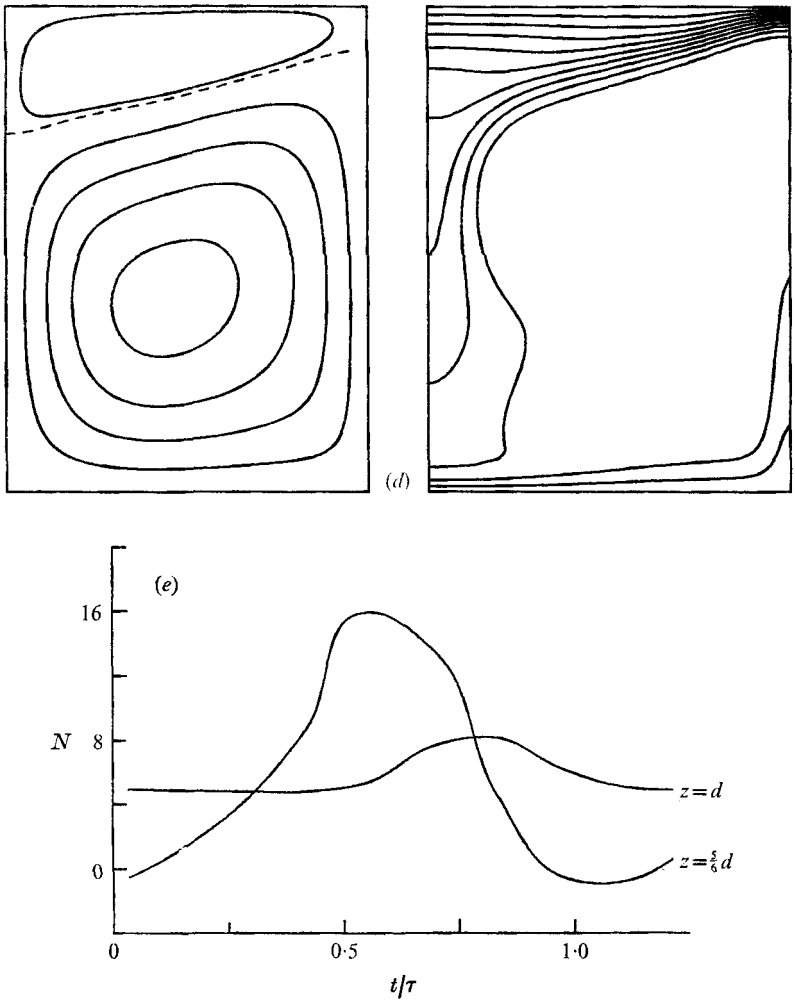

FIGURE 12. Time-dependent penetrative convection, $\lambda = 3$, $R = 42R_c$. Streamlines and isotherms are shown for times (*a*) $t/\tau = \frac{1}{4}$, (*b*) $t/\tau = \frac{1}{2}$, (*c*) $t/\tau = \frac{3}{4}$, (*d*) $t/\tau = 1$, where τ is the period of the oscillation. The variation with time of the Nusselt number, evaluated at the levels $z = \frac{5}{6}d$ (where $z/d \approx \mu$) and $z = d$, is shown in (*e*). (The contours in (*a*)–(*d*) correspond to the times marked on the t axis in (*e*).)

R/R_c	N	Turnover time, τ_0'	Oscillation period τ'
7	3·7	24	25·2
14·1	4·6	22	22·0
21	5·2	20	10·0
28·2	5·7	20	10·0
42	4·8–8·4	21	10·5

TABLE 2. Periods for oscillatory convection ($\lambda = 3$, $l = \frac{3}{4}$). (Dimensionless times measured in units of $(d/g\alpha T_0^2)^{\frac{1}{2}}$.)

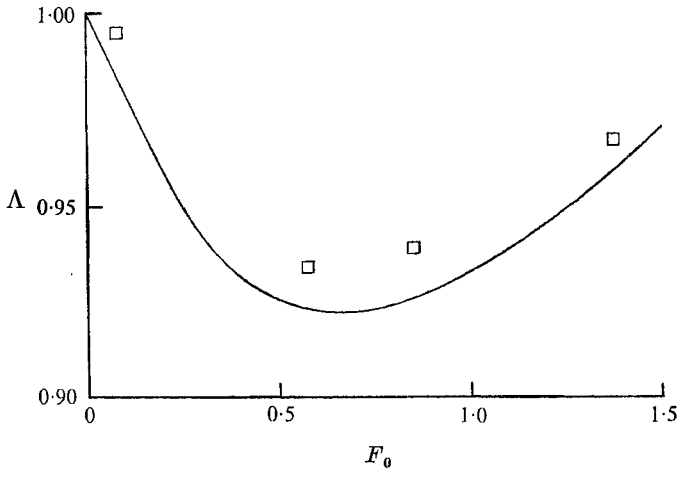

FIGURE 13. Penetrative convection with fixed flux at the lower boundary: variation of lower boundary temperature with heat flux. Plot of $\Lambda = (T_0 - T_L)/T_0$ as a function of $F_0 = Fd/(\kappa\lambda T_0)$. The points show results of numerical experiments with $\lambda = 3{\cdot}2$; the curve is computed from the simplified model. Points to the left of the minimum correspond to unstable convection in figure 11.

convected flux F_2 remains equal to the flux across the lower boundary, i.e. $dF_2/d\mu = 0$. But the change in the conducted flux $dF_1 = (dF_1/d\mu)\,d\mu$ and

$$dF_1/d\mu > 0.$$

Thus the interface will be restored to its original position and the system will be stable. Penetrative convection differs from the flow considered by Busse (1967*b*), which remained unstable with a fixed-flux boundary condition, thereby allowing nonlinear oscillations.

To investigate this problem we choose a Rayleigh number such that the cell with $T_L = 0$ °C is marginally stable, with flux $F_c = d/\kappa\lambda T_0$. We then increase the flux F across the lower boundary. Initially T_L increases to a maximum, after which it decreases monotonically; if we forget ice and allow $T_L < 0$ there exists a unique convecting solution for all $F > F_c$. It is convenient to describe these solutions in terms of $\Lambda = (T_0 - T_L)/T_0$ and $F_0 = F/F_c$. Computations were carried out with $\lambda = 3{\cdot}2$ and $1 \leqslant F_0 \leqslant 1{\cdot}4$. Λ decreased from 1 to 0·93 before rising again; in this range, $1 \leqslant N \leqslant 1{\cdot}2$ and $dN/dR < 0$, yet several steady convective solutions were found. Similar results were obtained with $\lambda \approx 2$. The simplified model can be applied to this problem too, by adapting the discussion in §2 so as to yield T_L as a function of F for a given value of R. The predicted values of Λ and F_0 are compared with those obtained from numerical experiments in figure 13. Once again, the agreement is satisfactory.

As an alternative to (50) the lower temperature can be kept at 0 °C while the mean flux is fixed at the upper boundary, so the thermal boundary conditions become

$$T = 0 \quad (z = 0), \quad \frac{d\overline{T}}{dz} = \text{constant} \quad (z = d), \quad \frac{\partial T}{\partial x} = 0 \quad (x = 0, L; z = d). \tag{51}$$

This change destabilizes the simplified model of penetrative convection: if the interface is displaced T_U will adjust itself so that F_1 is constant; then $dF_1 = 0$ while $dF_2/d\mu > 0$ and so the system is unstable. The layer must either be convective or conductive throughout. As the flux is increased from zero, the layer becomes unstable and convection carries more energy as T_U grows until $T_U = \gamma T_0$. This gives the maximum flux that can be carried by convection: thereafter, a rise in T_U would actually diminish the heat transport. If the flux is larger, it can only be carried by conduction; any increase in heat flux will, paradoxically, suppress convection.

7. Comparison with experiment

Two-dimensional convection between free boundaries may be computationally convenient and has some astrophysical relevance but laboratory experiments generate convection in regions with fixed boundaries. Moreover, the flow is three-dimensional, with cold fluid rising at the centres of hexagonal cells (Myrup *et al.* 1970). It is worth using the simplified model to predict the results of experiments. This can be done provided that the penetration factor γ and the function $\mathcal{N}$ can be estimated. To obtain this function we shall assume that $\mathcal{N}(R_E/R_{Ec})$ is the same as the corresponding function $\mathcal{N}(R/R_c)$ for Bénard convection between rigid boundaries. The latter has been determined experimentally by Rossby (1969).

In order to evaluate R_E/R_{Ec} we need to know both the critical Rayleigh number and the penetration factor γ; these can be estimated from the solution to the linearized problem (Veronis 1963). In fact this stability problem is identical to that for Couette flow between rotating cylinders (Debler 1966) and for $\lambda \gtrsim 2$ the critical Rayleigh number $R_c = 6{\cdot}06\pi^4\lambda^3$. To obtain the penetration factor we use the eigenfunction for $\lambda = 4$, which is given by Chandrasekhar (1961): the interface between the main cell and the counter cell, where the vertical velocity is zero, corresponds to a temperature $T_1 = 5{\cdot}5$ °C. For the linear problem, therefore, $\gamma = 1{\cdot}4$. With free boundaries the penetration factor was approximately the same for linear and nonlinear convection. So we shall assume that $\gamma = 1{\cdot}5$ for fixed boundaries also.

Townsend's (1964) experiment can be used to check the reliability of these assumptions. The heat flux and the effective Nusselt number are best determined from the measured value of $d\bar{T}/dz$ at $z = 0$. This can be taken from figure 4 of his paper and gives $N_E \approx 13{\cdot}6$. The effective Rayleigh number

$$R_E = 5{\cdot}3 \times 10^6 \quad \text{and} \quad R_{Ec} = 2{\cdot}0 \times 10^3.$$

Thus $R_E/R_{Ec} = 2{\cdot}7 \times 10^3$. But from Rossby's experiments on Bénard convection in water $N = 13$ when $R/R_c = 2{\cdot}7 \times 10^3$. The agreement between this value and the measured value of N_E supports the various assumptions made above.

The model can now be used to predict the Nusselt number for penetrative convection. Instead of the curve for $\mathcal{N}(R/R_c)$ in figure 9, we use that given by Rossby. For $\lambda \leqslant 1{\cdot}5$, $N(R/R_c)$ will be given by this curve, which is plotted in figure 14 for $\lambda = 1$. Values of N for penetrative convection can be estimated

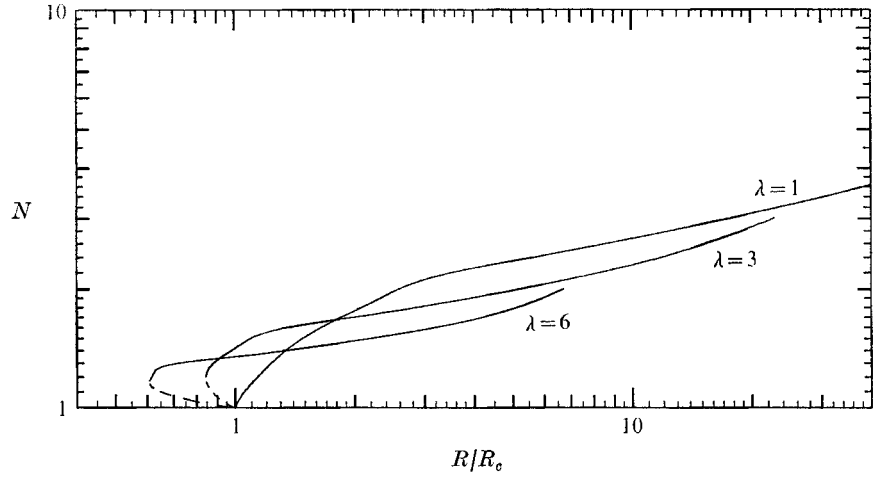

FIGURE 14. Penetrative convection between fixed boundaries. Values of N as a function of R/R_c for experiments using water with $\lambda = 1, 3, 6$, predicted from the simplified model, together with Rossby's (1969) results for Bénard convection.

from the model by using a transparency of this curve as before and results for $\lambda = 3$ and 6 are also shown in figure 14. The nonlinear instability once again allows convection at subcritical Rayleigh numbers and details are given in table 1. As might be expected, finite amplitude convection is apparently inhibited by the more stringent boundary conditions. The curves of $N(R/R_c)$ are more complicated than those in figure 11. This is partly caused by the knee at $R \approx 10R_c$ in Rossby's curve, corresponding to the transition from rolls to three-dimensional convection (Busse 1967*a*; Busse & Whitehead 1971): however this transition should not occur for penetrative convection, where hexagons will be preferred from the start (Busse 1967*c*).

Furumoto & Rooth (1961) found that $N \approx 1{\cdot}1\ (R/R_c)^{\frac{1}{3}}$ (Malkus 1963), which is consistent with the results in figure 11, where $N \propto R^{0{\cdot}3}$ for $R \gtrsim 4R_c$. The experiments of Townsend (1964) and Myrup *et al.* (1970) were carried out in square boxes of width $2d$ and d respectively, so that lateral heat losses were large enough to preclude exact comparison with predictions from our model. They found a temperature of 3·2 °C in most of the convective region, as compared with 2·5 °C in our numerical experiments with free boundaries; this discrepancy is probably caused by the difference in boundary conditions. Measurements made by Furumoto & Rooth indicated the presence of counter cells in the stable region (Veronis 1963). At high Rayleigh numbers gravity waves should predominate in this region and no counter cells were observed by Townsend or Myrup *et al.* The nonlinear instability has not yet been thoroughly investigated and we hope that the discussion and calculations in this paper may stimulate further experiments on the ice-water problem.

8. Conclusion

The ice-water experiment provides an example of an essentially nonlinear fluid-dynamical problem whose behaviour can be understood and described in simple terms. We have investigated steady two-dimensional penetrative convection between free boundaries numerically in some detail. Time-dependent behaviour has also been explored, together with the effect of different boundary conditions. We have extended Musman's (1968) analysis to construct a simplified model which gives a quantitative understanding of penetrative convection. Predictions from this model were verified by the numerical results and can easily be adapted to fit other versions of the experiment.

Penetration of convection into a stable layer has also been investigated in a number of related problems (Spiegel 1972). The temperature gradient can be altered by changing the boundary temperatures (Krishnamurti 1968*a*, *b*; Deardorff, Willis & Lilly 1969) or else by heating (Whitehead & Chen 1970) or cooling (Faller & Kaylor 1970) from within, so that non-uniform gradients affect heat flow rather than momentum. In these experiments convection is always found to be three-dimensional and dominated by penetrating plumes. The jets found by Whitehead & Chen (1970) correspond to the narrow rising plumes of Myrup *et al.* (1970) and may penetrate further than is indicated by two-dimensional calculations (Latour 1973).

This paper has concentrated on convection in a fluid with the properties of water around 4 °C. Spiegel (1972) reviews the relevance of penetrative convection to a variety of natural phenomena. The ice-water problem may serve as a guide to compressible models of convective zones in stars (Latour 1973) though these zones are contained between two sub-adiabatically stratified layers. A more relevant Boussinesq model for stellar convection can be obtained by assuming a cubic dependence of density on temperature such that a central unstable region floats between two stable layers.

The extent of the penetration of motion into the stable layers is of some importance, since the anomalous depletion of lithium in late-type stars might be explained if convection penetrates deep enough for the reaction Li (p, α) He to occur (Bodenheimer 1965; Spiegel 1968). Linear modes have been computed for the sun (Böhm 1963, 1967; Kohl 1966) and our results indicate that linear theory provides a qualitatively correct estimate of the extent of penetration. However, the nature of penetrative convection depends on the value of the Prandtl number. Numerical experiments on floating convection and on the effect of varying the Prandtl number will form a separate investigation.

Our time-dependent computations show that penetrative convection can excite oscillations in the stable region above. The oscillations with a period of 300 s observed in the solar photosphere could be trapped gravitational waves (Simon 1972, private communication; Thomas 1972; Thomas, Clark & Clark 1971); however, they are more likely to be excited randomly, as in Townsend's experiment, than by direct coupling as in our model. Further work is needed on the behaviour of individual thermals impinging on a stable region (Moore 1967)

both in this context and as a description of behaviour at the tropopause (Townsend 1966) and in the ocean.

D.R.M. is grateful to the Marshall Aid Commemoration Commission and the National Science Foundation for scholarships held while this work was being done. The computations were carried out on the IBM 360/44 computer at the Institute of Astronomy, Cambridge and the 360/91 computer at the Institut für Plasmaphysik, Garching. We wish to thank Dr S. Musman for informative discussion and correspondence on this problem. We are also grateful for comments from Professor W. A. Fowler, Dr D. O. Gough, Dr K. von Sengbusch, Dr H. U. Schmidt and Dr E. A. Spiegel. This paper was written at the Max-Planck-Institut für Astrophysik, Munich.

REFERENCES

BATCHELOR, G. K. 1967 *An Introduction to Fluid Dynamics.* Cambridge University Press.

BODENHEIMER, P. 1965 *Astrophys. J.* **142**, 451.

BÖHM, K.-H. 1963 *Astrophys. J.* **138**, 297.

BÖHM, K.-H. 1967 In *Aerodynamic Phenomena in Stellar Atmospheres* (ed. R. N. Thomas), p. 366. Academic.

BUSSE, F. H. 1967*a* *J. Math. & Phys.* **46**, 140.

BUSSE, F. H. 1967*b* *J. Fluid Mech.* **28**, 223.

BUSSE, F. H. 1967*c* *J. Fluid Mech.* **30**, 625.

BUSSE, F. H. & WHITEHEAD, J. A. 1971 *J. Fluid Mech.* **47**, 305.

CHANDRASEKHAR, S. 1961 *Hydrodynamic and Hydromagnetic Stability*, chap. 2. Clarendon Press.

DEARDORFF, J. W. 1964 *J. Atmos. Sci.* **21**, 419.

DEARDORFF, J. W., WILLIS, G. E. & LILLY, D. K. 1969 *J. Fluid Mech.* **35**, 7.

DEBLER, W. R. 1966 *J. Fluid Mech.* **24**, 165.

ELDER, J. W. 1969 *J. Fluid Mech.* **35**, 417.

FALLER, A. J. & KAYLOR, R. 1970 *J. Geophys. Res.* **75**, 521.

FROMM, J. E. 1965 *Phys. Fluids*, **8**, 1757.

FURUMOTO, A. & ROOTH, C. 1961 Geophysical fluid dynamics. *Woods Hole Oceanographic Inst. Rep.*

HERRING, J. R. 1963 *J. Atmos. Sci.* **20**, 325.

KOHL, K. 1966 *Z. Astrophys.* **64**, 472.

KRISHNAMURTI, R. 1968*a* *J. Fluid Mech.* **33**, 445.

KRISHNAMURTI, R. 1968*b* *J. Fluid Mech.* **33**, 457.

LAMB, H. 1932 *Hydrodynamics.* Cambridge University Press.

LATOUR, J. 1973 To be published.

MALKUS, W. V. R. 1960 In *Aerodynamical Phenomena in Stellar Atmospheres* (ed. R. N. Thomas), p. 346. Bologna: Zanichelli.

MALKUS, W. V. R. 1963 *Proc. 3rd Tech. Conf. on Hurricanes & Tropical Met.*, p. 89. Mexico.

MOORE, D. R., PECKOVER, R. S. & WEISS, N. O. 1973 Difference methods for time-dependent two-dimensional convection. *Comp. Phys. Comm.* (in press).

MOORE, D. R. & WEISS, N. O. 1973 *J. Fluid Mech.* **58**, 289.

MOORE, D. W. 1967 In *Aerodynamic Phenomena in Stellar Atmospheres* (ed. R. N. Thomas), p. 405. Academic.

MUSMAN, S. 1968 *J. Fluid Mech.* **31**, 343.

MYRUP, L., GROSS, D., HOO, L. S. & GODDARD, W. 1970 *Weather*, **25**, 150.

ROSSBY, H. T. 1969 *J. Fluid Mech.* **36**, 309.

SPIEGEL, E. A. 1967 In *Aerodynamic Phenomena in Stellar Atmospheres* (ed. R. N. Thomas), p. 348. Academic.

SPIEGEL, E. A. 1968 *Highlights of Astronomy* (ed. L. Perek), p. 261. Dordrecht: Reidel.

SPIEGEL, E. A. 1971 *Ann. Rev. Astron. Astrophys.* **9**, 323.

SPIEGEL, E. A. 1972 *Ann. Rev. Astron. Astrophys.* **10**, 261.

THOMAS, J. H. 1972 *Solar Phys.* **24**, 262.

THOMAS, J. H., CLARK, P. A. & CLARK, A. 1971 *Solar Phys.* **16**, 51.

TOWNSEND, A. A. 1964 *Quart. J. Roy. Met. Soc.* **90**, 248.

TOWNSEND, A. A. 1966 *J. Fluid Mech.* **24**, 307.

VERONIS, G. 1963 *Astrophys. J.* **137**, 641.

VERONIS, G. 1965 *J. Mar. Res.* **23**, 1.

VERONIS, G. 1966*a* *J. Fluid Mech.* **24**, 545.

VERONIS, G. 1966*b* *J. Fluid Mech.* **26**, 49.

VERONIS, G. 1968*a* *J. Fluid Mech.* **31**, 113.

VERONIS, G. 1968*b* *J. Fluid Mech.* **34**, 315.

WELANDER, P. 1967 *J. Fluid Mech.* **29**, 17.

WHITEHEAD, J. A. & CHEN, M. M. 1970 *J. Fluid Mech.* **40**, 549.